The Astrophysical Journal Letters, 908:L39 (6pp), 2021 February 20 https://doi.org/10.3847/2041-8213/abdf64
© 2021. The American Astronomical Society. All rights reserved.

Heavy Elements Unveil the Non-primordial Origin of the Giant H I Ring in Leo

Edvige Corbelli[1], Giovanni Cresci[1], Filippo Mannucci[1], David Thilker[2], and Giacomo Venturi[1,3]
[1] INAF-Osservatorio di Arcetri, Largo E. Fermi 5, I-50125 Firenze, Italy; edvige.corbelli@inaf.it
[2] Department of Physics and Astronomy, The Johns Hopkins University, Baltimore, MD, USA
[3] Instituto de Astrofísica, Facultad de Física, Pontificia Universidad Católica de Chile, Casilla 306, Santiago 22, Chile
Received 2020 November 30; revised 2021 January 18; accepted 2021 January 21; published 2021 February 22

Abstract

The origin and fate of the most extended extragalactic neutral cloud known in the local universe, the Leo ring, is still debated 38 yr after its discovery. Its existence is alternatively attributed to leftover primordial gas with some low level of metal pollution versus enriched gas stripped during a galaxy−galaxy encounter. Taking advantage of Multi Unit Spectroscopic Explorer operating at the Very Large Telescope, we performed optical integral field spectroscopy of three H I clumps in the Leo ring where ultraviolet continuum emission has been found. We detected, for the first time, ionized hydrogen in the ring and identify four nebular regions powered by massive stars. These nebulae show several metal lines ([O III], [N II], [S II]) that allowed reliable measures of metallicities, found to be close to or above the solar value ($0.8 \leqslant Z/Z_{\odot} \leqslant 1.4$). Given the faintness of the diffuse stellar counterparts, less than 3% of the observed heavy elements could have been produced locally in the main body of the ring and not much more than 15% in the H I clump toward M96. This inference, and the chemical homogeneity among the regions, convincingly demonstrates that the gas in the ring is not primordial, but has been pre-enriched in a galaxy disk, then later removed and shaped by tidal forces and it is forming a sparse population of stars.

Unified Astronomy Thesaurus concepts: Chemical abundances (224); Intergalactic clouds (809); Interacting galaxies (802); H II regions (694)

1. Introduction

The serendipitous discovery of an optically dark H I cloud in the M96 galaxy group (Schneider et al. 1983), part of the Leo I group, has since triggered much discussion on the origin and survival of the most massive and extended intergalactic neutral cloud known in the local universe ($D \leqslant 20$ Mpc). With an extension of about 200 kpc and an H I mass $M_{\rm H\ I} \simeq 2 \times 10^9$ $M_{\odot}$, the cloud has a ring-like shape orbiting the galaxies M105 and NGC 3384 (Schneider 1985), and it is known also as the Leo ring. As opposed to tidal streams, the main body of the Leo ring is isolated, more distant than 3 optical radii from any luminous galaxy. The ring is much larger than any known ring galaxy (Ghosh & Mapelli 2008). The collisional ring of NGC 5291 ($D \simeq 50$ Mpc; Longmore et al. 1979; Boquien et al. 2007), of similar extent, is vigorously forming stars, as many other collisional rings. The Leo ring is much more quiescent and for many years since its discovery has been detected only via H I emission. Lacking a pervasive optical counterpart (Kibblewhite et al. 1985; Pierce & Tully 1985; Watkins et al. 2014), it has been proposed as a candidate primordial cloud (Schneider et al. 1989; Sil'chenko et al. 2003) dating to the time of the Leo I group formation.

The bulk of the H I gas in the ring is on the south and west side, especially between M96 (to the south) and NGC 3384/M105 (at the ring center; see Figure 1). Intermediate-resolution Very Large Array (VLA) maps of this region with an effective beam of 45″ revealed the presence of gas clumps (Schneider et al. 1986), some of which appear as distinct virialized entities and have masses up to 3.5×10^7 $M_{\odot}$. The position angle of the clump major axes and their velocity field suggest some internal rotation with a possible disk-like geometry and gas densities similar to those of the interstellar medium. Distinct cloudlets are found in the extension pointing south, toward M96. Detection of GALEX ultraviolet (UV)-continuum light in the direction of a few H I clumps of the ring suggested star formation activity between 0.1 and 1 Gyr ago (Thilker et al. 2009). However, most of the gas mass is not forming massive stars today because there has been no confirmed diffuse Hα emission (Reynolds et al. 1986; Donahue et al. 1995) or CO detection from a pervasive population of giant molecular complexes (Schneider et al. 1989).

A low level of metal enrichment, inferred from GALEX-UV and optical colors, favored the primordial origin hypothesis. This was supported a few years later by the detection of weak metal absorption lines in the spectra of three background quasi-stellar objects (QSOs), two of which have sightlines close or within low H I column density contours of the ring (Rosenberg et al. 2014). However, the low metallicity, estimated between 2% and 16% solar for Si/H, C/H, and N/H, has large uncertainties due to ionization corrections. Confusion with emission from the Milky Way in the QSO's spectra does not allow to measure H I column densities along the sightlines. This is inferred from large-scale H I gas maps, and gas substructures on small scales can alter the estimated abundance ratios.

The Leo ring has also been considered as a possible product of a gas-sweeping head-on collision (Rood & Williams 1985), involving group members such as NGC 3384 and M96 (Michel-Dansac et al. 2010) or a low surface brightness galaxy colliding with the group (Bekki et al. 2005). A tentative detection of dust emission at 8 μm in one H I clump (Clump1; Bot et al. 2009) also supports the pre-enrichment scenario. A direct and reliable measurement of high-metallicity gas associated to the very weak stellar counterpart can give the conclusive signature of a ring made of pre-enriched gas.

In this Letter we present the first detection of nebular regions in the Leo ring. In Section 2 we describe integral field optical spectroscopy of three fields in the ring and estimate metal abundances from emission lines in star-forming regions. The local metal production and the implications for the origin of the

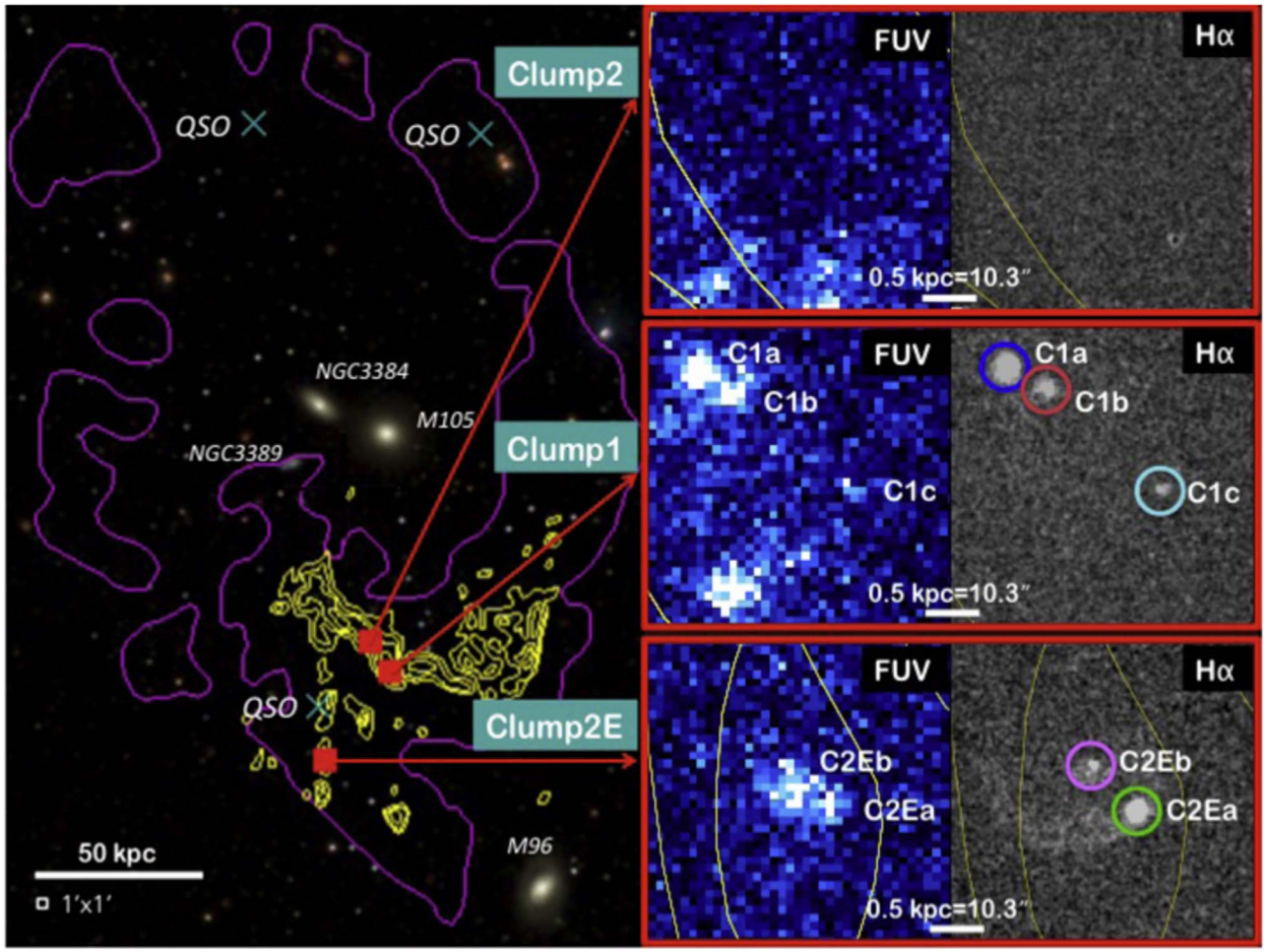

Figure 1. Left panel: H I contours of the Leo ring are overlaid to the optical image of the M96 group (Sloan Digital Sky Survey (SDSS) color image). In magenta the Arecibo contour at $N_{\rm H\,I} = 2 \times 10^{18}$ cm^{-2}, in yellow the VLA H I contours of the southern part of the ring Schneider et al. (1986). Crosses indicate background quasi-stellar objects (QSOs; Rosenberg et al. 2014), and red squares indicate the H I clumps observed with the Multi Unit Spectroscopic Explorer (MUSE): Clump1(C1), Clump2(C2), and Clump2E(C2E). The 1 arcmin^2 angular size of the MUSE field is shown in the bottom-left corner. Right panels: MUSE Hα images of Clump1 and of Clump2E show the five nebular regions detected. The corresponding GALEX-far-ultraviolet (FUV) continuum emission is displayed to the left of the Hα images. The southernmost FUV source in the field of Clump1 is a background galaxy.

Leo ring are discussed in the last Section. In a companion paper (Corbelli et al. 2021; hereafter Paper II) we analyze star formation and the stellar population in and around the detected nebulae using GALEX and Hubble Space Telescope (HST) images.

2. The Discovery of Nebular Regions and Their Chemical Abundances

We assume a distance to the Leo ring of 10 Mpc, as for M96 and M105. This implies that an angular separation of 1″ corresponds to a spatial scale of 48.5 pc.

2.1. The Data

Between 2019 December and 2020 March we have observed three 1×1 arcmin^2 regions in the Leo ring using the integral field spectrograph Multi Unit Spectroscopic Explorer (MUSE) mounted on the European Space Agency (ESO) Very Large Telescope (VLT). The locations of MUSE fields are shown in red in the left panel of Figure 1 overlaid on the Sloan Digital Sky Survey (SDSS) optical image of the M96 group and on the VLA H I contours of the ring. The fields have been centered at three H I peak locations, Clump1, Clump2, and Clump2E, two in the main body of the ring and one in the filament connecting the ring to M96. They cover completely the UV-bright regions of Clump1 and Clump2E listed by Thilker et al. (2009). The southernmost side of the UV emission in Clump2 is at the border of the MUSE field.

The final cube for each region is the result of two observing blocks, one totaling 960 s and the other 1920 s. The observing blocks are a combination of two and four 480 s exposures, respectively, which were rotated and dithered from each other in order to provide a uniform coverage of the field and to limit systematics. Dedicated offset sky exposure of 100 s each were acquired every two object exposures. The reduction of the raw data was performed with the ESO MUSE pipeline (Weilbacher et al. 2020), which includes the standard procedures of bias subtraction, flat-fielding, wavelength calibration, flux calibration, sky subtraction, and the final cube reconstruction by the spatial arrangement of the individual slits of the image slicers. For Clump1 we did not employ the dedicated sky observations for the sky subtraction, as these were giving strong sky residuals, especially around the Hα line. We thus extracted the sky spectrum to be subtracted from within the science cube, by selecting the portions of the field of view (FoV) free of source emission. This allowed to remove the problematic sky residuals

Table 1
H II Region Coordinates, Chemical Abundance, and Extinction

Source	R.A.	Decl.	$V_{\rm hel}$ (km s^{-1})	12+log(O/H)	A_V (mag)	$Z/Z_\odot$	$R_{\rm ap}^{\rm max}$ (arcsec)	$A_{H\alpha}^{R\,\rm max}$ (mag)	log $L_{\rm H\alpha}$ (erg s^{-1})
C1a	10:47:47.93	12:11:31.9	994 ± 2	$8.59^{+0.04}_{-0.04}$	$1.02^{+0.60}_{-0.60}$	0.79	5.0	0.40	36.62
C1b	10:47:47.44	12:11:27.6	1003 ± 3	$8.63^{+0.28}_{-0.04}$	$0.06^{+1.59}_{-0.06}$	0.87	3.0	…	35.94
C2Ea	10:48:13.52	12:02:24.3	940 ± 3	$8.84^{+0.01}_{-0.01}$	$0.47^{+0.31}_{-0.35}$	1.41	3.4	0.61	36.91
C2Eb	10:48:14.08	12:02:32.5	937 ± 21	$8.82^{+0.09}_{-0.11}$	…	1.35	3.0	…	35.85

Note. Extinction-corrected total Hα luminosities are computed using circular apertures with radius $R_{\rm ap}^{\rm max}$.

Table 2
Integrated Emission for Gaussian Fits to Nebular Lines with $R_{\rm ap} = 1\farcs2$

Source	Hβ	[O III]5007	[N II]6548	Hα	[N II]6583	[S II]6716/	[S II]6731	FWHM$_{b,r}$[Å]
C1a	1.89 ± 0.37	1.53 ± 0.38	<0.46	7.89 ± 0.29	1.39 ± 0.25	0.86 ± 0.21	0.54 ± 0.21	2.5,2.5
C1b	1.00 ± 0.37	<0.76	<0.49	3.17 ± 0.23	0.82 ± 0.31	<0.40	<0.40	1.9,2.2
C2Ea	7.97 ± 0.41	1.34 ± 0.37	3.88 ± 0.31	26.57 ± 0.35	11.39 ± 0.36	2.71 ± 0.33	1.81 ± 0.36	2.8,2.4
C2Eb	<0.79	<0.79	<0.76	2.25 ± 0.35	1.01 ± 0.32	<0.34	<0.34	…, 2.1

Note. Upper limits are 3σ values, flux units are 10^{-17} erg s^{-1} cm^{-2}.

because the sky spectrum obtained from within the science FoV is simultaneous with the science spectra. The final data set comprises three data cubes, one per clump, covering a FoV slightly larger than 1 arcmin^2. Each spectrum spans the wavelength range 4600–9350 Å, with a typical spectral resolution between 1770 at 4800 Å and 3590 at 9300 Å. The spatial resolution given by the seeing is of the order of 1″.

2.2. H II Regions in the Ring

We analyze spectral data at the observed spectral and spatial resolution searching for Hα emission at the velocities of the H I gas in the ring i.e., between 860 and 1060 km s^{-1}. We detect hydrogen and some collisionally excited metal lines in three distinct regions of Clump1 (C1a, C1b, C1c) and in two regions of Clump2E (C2Ea, C2Eb). Figure 1 shows the GALEX-FUV continuum and the Hα emission in the three MUSE fields. The FUV emission in Clump2E seems more extended than the H II region in Hα and suggests a non-coeval population or the presence of some low-mass stellar cluster lacking massive stars. No nebular lines are detected in the field covering Clump2. This clump is the reddest of the three clumps observed, having the largest values of UV and optical colors (Thilker et al. 2009; Watkins et al. 2014).

The four regions listed in Table 1 are H II regions associated with recent star formation events according to their line ratios (Kauffmann et al. 2003; Sanders et al. 2012) and to the underlying stellar population (see Paper II). The data relative to the faintest nebula detected, C1c, is presented and discussed in Paper II because emission line ratios and [O III]5007 luminosity are consistent with the object being a planetary nebula whose metallicity is unconstrained due to undetected lines. We give in Table 1 the central coordinates of the H II regions and the mean recession velocities of identified optical lines. These are consistent with the 21 cm line velocities of the H I gas (Schneider et al. 1986). We fit Gaussian profiles to emission lines whose peaks are well above 3σ in circular apertures with radius 1″.2, comparable to the seeing. With these apertures we sample more than one-third of the region total Hα luminosity and achieve good signal-to-noise ratio (S/N > 2.5) for integrated Gaussian line fits to all detected lines. The integrated line fluxes are shown in Table 2. We require a uniform Gaussian line width in the red or in the blue part of the spectrum because lines are unresolved. The resulting FWHM are shown in Table 2. Upper limits in Table 2 are 3σ values for non-detected lines, inferred using the rms of the spectra at the expected wavelength and a typical full spectral extent of the line. For the brightest H II regions we detected strong metal lines, such as [O III]5007, [N II]6583, [S II]6716,6731 which can be used to compute reliable metallicities.

2.3. Chemical Abundances

For the four H II regions in Table 1 we compute the gas-phase metal abundances using the strong line calibration in Curti et al. (2020). All the available emission lines and the upper limits to the undetected lines are used to measure metallicity and dust extinction in a two-parameter minimization routine, which also estimates the uncertainties on these two parameters. The resulting metal abundances are displayed in Figure 2 and in Table 1. In Figure 2 we show the 1σ confidence levels in the oxygen abundance-visual extinction plane and the best-fitting values of chemical abundances along the calibration curves for the strong line ratios. Line ratios for all the H II regions are well reproduced by close to solar metallicities and moderate visual dust extinctions. For C2Eb, extinction cannot be constrained. Metallicities in Clump1 are slightly below solar, while those in Clump 2E are above solar. The H II regions in Clump 1 have lower S II/Hα line ratios than predicted by Curti et al. (2020). This is also found in outer disk H II regions (Vilchez & Esteban 1996) and it is likely due to a high ionization parameter driven by a low-density interstellar medium (Dopita et al. 2013). The mass fraction of metals with respect to solar, $Z/Z_\odot$, ranges between 0.79 and 1.41 (assuming solar distribution of heavy elements and $Z_\odot = 0.0142$; Asplund et al. 2009).

Using wide apertures, as listed in column (8) of Table 1 and chosen to include most of Hα emission with no overlap, we derive the H II region total Hα luminosities, $L_{\rm H\alpha}$. These are given in column (10) already corrected for extinction when this can be estimated from the Balmer decrement in these apertures (column (9)). Luminosities are high enough to require the

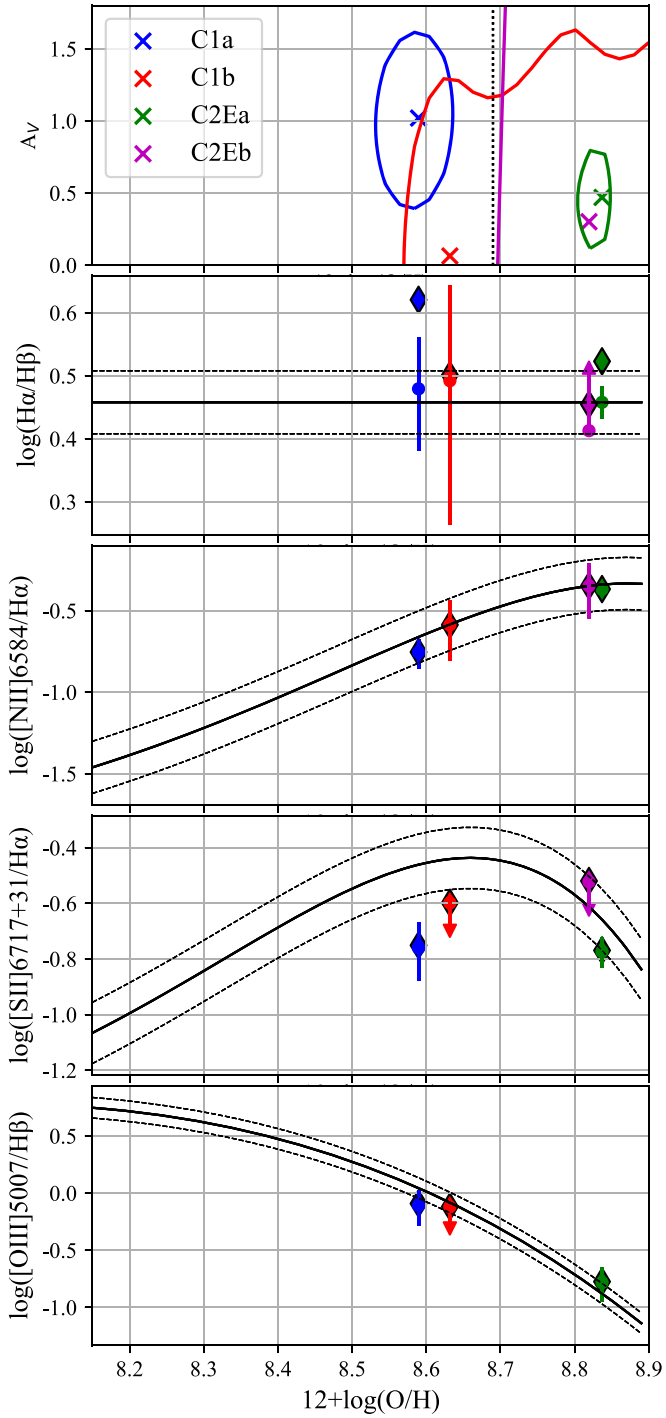

Figure 2. Dust visual extinction and gas-phase metallicity for each H II region, color-coded as in the legend. In the top panel we show the best-fitting values (cross) and 1σ confidence levels of A_V; the dotted line shows the solar metallicity ($12 + \log(\mathrm{O/H}) = 8.69$). The four bottom panels refer to relevant strong line ratios. Diamonds show the observed values of the line ratio plotted at the best-fitting value of metallicity. The $\mathrm{H}\alpha/\mathrm{H}\beta$ ratio is computed for Case B recombination with uncertainties due to the unknown temperature, and circles showing extinction-corrected values. The solid curves in the lower three panels trace the calibrations from Curti et al. (2020), with the relative uncertainties.

presence of very massive and young stars, especially for C1a and C2Ea. The local production rate of ionizing photons by hot stars might be higher than what can be inferred using $L_{\mathrm{H}\alpha}$ if some photons leak out or are directly absorbed by dust in the nebula.

The H II regions in the [O III]/Hβ versus [N II]/Hα plane, known as the Baldwin, Phillips & Terlevich (BPT) diagram (Baldwin et al. 1981), are consistent with data from young H II regions in galaxies (Kauffmann et al. 2003; Sanders et al. 2012) and their metallicities are in agreement with those predicted by photoionization models of H II regions (Dopita et al. 2013; Byler et al. 2017). Line ratios observed in Clump1 are also consistent with the distribution of the recent evolution models of H II regions in gas clouds (Pellegrini et al. 2020), available only for solar metallicity. These predict an age of about 5 Myr for C1a. Line ratios for C2Ea instead fall outside the area where solar metallicity H II regions are found, in agreement with the higher than solar metallicity that we infer for this clump. A very young age is recovered in Paper II for this H II region through a multiwavelength analysis.

3. In Situ Metal Enrichment and the Ring Origin

We compute the maximum mass fraction of metals that could conceivably be produced in situ, $f_Z^{\max}$, given the observed metal abundances, Z_{obs}, and the limiting blue magnitudes of the Leo ring, μ_B. For this extreme local enrichment scenario we assume that all stars have formed in the ring and use the instantaneous burst or continuous star formation models of Starburst99 (Leitherer et al. 1999) in addition to population synthesis models of Bruzual & Charlot (2003) for an initial burst with an exponential decay ($\tau = 1$ Gyr). At each time step we compute the $B - V$ color and the maximum stellar surface mass density that corresponds to the limiting values of μ_B. This stellar density gives the maximum mass fraction of metals produced locally. In order to maximize the local metal production we consider a closed box model with no inflows or outflows for which a simple equation relates the stellar yields to the increase in metallicity since star formation has switched on (Searle & Sargent 1972):

$$f_Z^{\max} = \frac{Z}{Z_{\mathrm{obs}}} = \frac{y_Z}{Z_{\mathrm{obs}}} \ln\left(\frac{\Sigma_{g0}}{\Sigma_g}\right) = \frac{y_Z}{Z_{\mathrm{obs}}} \ln\left(1 + \frac{\Sigma_*}{\Sigma_g}\right) \quad (1)$$

where Z and Σ_* are the abundance of metals by mass and the stellar mass surface density produced in situ. The gas mass surface density at the present time and at the time of the Leo ring formation are Σ_g and Σ_{g0}, respectively. The total net yields y_Z refers to the mass of all heavy elements produced and injected into the interstellar medium by a stellar population to the rate of mass locked up into low-mass stars and stellar remnants. There are several factors that can affect the yields: the upper end of the initial mass function (IMF), massive star evolution and ejecta models, and metallicity. Since the pioneer work of Searle & Sargent (1972) several papers have analyzed these dependencies (e.g., Maeder 1992; Meynet & Maeder 2002; Romano et al. 2010; Vincenzo et al. 2016). Following the results of Romano et al. (2010), Vincenzo et al. (2016), we consider negligible the metallicity dependence on the yields and consider the Chabrier IMF i.e., an IMF with a Salpeter slope from $1\,M_\odot$ up to its high-mass end at $100\,M_\odot$ and a Chabrier-lognormal slope from 0.1 to $1\,M_\odot$ (Salpeter 1955; Chabrier 2003). This IMF has a total yield $y_Z = 0.06$, the highest among commonly considered IMF (Vincenzo et al. 2016).

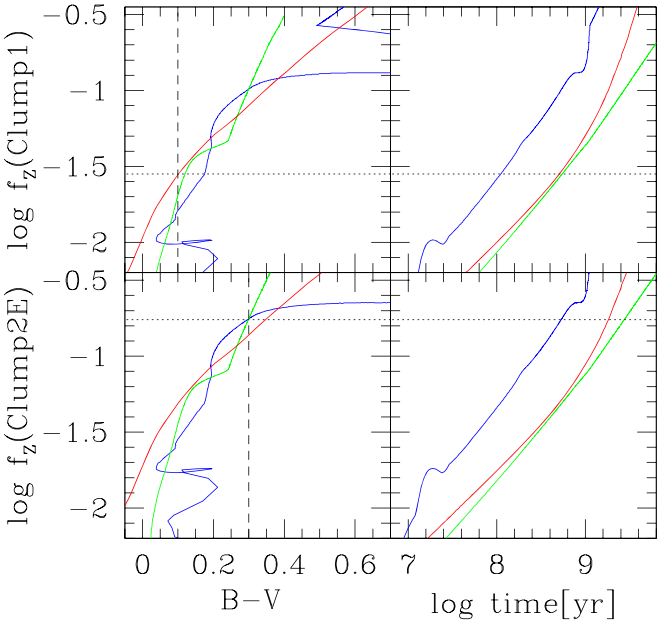

Figure 3. Mass fraction of metals f_Z produced in situ for an instantaneous burst (blue lines), a burst with exponential decay (red lines), and a continuous star formation model (green lines) as a function of optical colors (left panels) and time (right panels). Each model for both Clump1 (top panels) and Clump2E (bottom panels) is normalized as to produce an apparent magnitude $\mu_B = 29$ at any time after star formation switches on. The dashed lines indicate the maximum $B-V$ optical color of the clumps, and the dotted line $f_Z^{\max}$, the highest value of f_Z compatible with $B-V$.

To maximize the associated fraction of metals produced locally, $f_Z^{\max}$, we consider zero extinction and the best-fitted metallicities for C1a and C2Ea minus 3 times their dispersion, i.e., $Z_{\rm obs} = 0.6$ and $1.32\,Z_\odot$ for Clump1 and Clump2E, respectively. A very large fraction of the H I rich ring area corresponding to the VLA coverage of Schneider et al. (1986) has been surveyed deeply in the optical B-band (Pierce & Tully 1985; Watkins et al. 2014). For a very diffuse pervasive population throughout the Leo ring the survey results give $\mu_B \geqslant 30$ mag arcsec^{-2}. For optical emission in less extended regions as the MUSE fields, or equivalently at the VLA H I map spatial resolution (Schneider et al. 1986), and following the results of Mihos et al. (2018) we can use the more conservative upper limit $\mu_B \geqslant 29$ mag arcsec^{-2}. Given the optical colors $B-V = 0.0 \pm 0.1$ for Clump1 and $B-V = 0.1 \pm 0.2$ mag for Clump2E (Watkins et al. 2014), we consider $B-V \leqslant 0.1$ and $B-V \leqslant 0.3$ for Clump1 and Clump2E, respectively. The average H I + He gas surface density over a circular area with 45″ radius is $\Sigma_g = 3.1$ and $0.8\,M_\odot$ pc^{-2} in Clump1 and Clump2E, respectively. We compute from the models the stellar mass surface density corresponding to $\mu_B = 29$ mag arcsec^{-2} at each time, and f_Z with the above values of Σ_g, $Z_{\rm obs}$ and y_Z, using Equation (1). The value of $f_Z^{\max}$ will be f_Z at the maximum value of $B-V$ for each clump. In Figure 3 we show f_Z for the three models as a function of time and of $B-V$. The dashed line indicates the limiting value of $B-V$. A dotted line has been placed at the value of $f_Z^{\max}$ i.e., where the limiting colors intersect the models that produce the highest mass of metals.

For Clump1 a starburst 500 Myr ago that slowly decays with time gives the highest possible local metal production with $f_Z^{\max} = 3\%$ and $\Sigma_* = 0.01\,M_\odot$ pc^{-2}. For Clump2E both an instantaneous burst 500 Myr ago or a continuous star formation since 2 Gyr ago gives the maximum value of $f_Z^{\max} = 17\%$ with $\Sigma_* = 0.04\,M_\odot$ pc^{-2}. We conclude that the fraction of metals produced locally is too small to be compatible with a scenario of a primordial metal-poor ring enriched in situ. The ring must have formed out of metal-rich gas, with chemical abundances above $0.5\,Z_\odot$, mostly polluted while residing in a galaxy and then dispersed into space.

We underline that all models predict a small fraction of metals produced in situ and that the ones that maximize f_Z are not necessarily the best-fitted models to the underlying stellar population. These will be examined in Paper II. The apparent discrepancy between our results and the lower abundances inferred by the QSO's absorption lines can be resolved if hydrogen column densities along sightlines to nearby QSOs are lower than those used in the analysis of Rosenberg et al. (2014) and estimated from H I emission averaged over a large beam. The most discrepant abundance with respect to the nearly solar abundances that we infer for the ring is for carbon toward the southernmost QSO: $-1.7 \leqslant [{\rm C/H}]/[{\rm C/H}]_\odot \leqslant -1.1$. If future measures of the H I column density toward the QSO's sightline confirm the low metal abundances, these can be used to investigate chemical inhomogeneities due to a mix of metal-rich gas with local intragroup metal-poor gas in the ring outskirts.

We summarize that our finding has confirmed spectroscopically the association between stellar complexes detected in the UV-continuum and the high column density gas (Thilker et al. 2009). The detected Hα emission implies a sporadic presence of a much younger and massive stellar population than estimated previously (see Paper II for more details). For the first time we have detected gaseous nebulae in the ring with chemical abundances close to or above solar that conflict with the primordial origin hypothesis of the Leo ring. A scenario of pre-enrichment, where the gas has been polluted by the metals produced in a galaxy and subsequently tidally stripped and placed in ring-like shape, is in agreement with the data presented in this Letter. This picture is dynamically consistent with numerical simulations showing the possible collisional origin of the Leo ring (Bekki et al. 2005; Michel-Dansac et al. 2010) and with chemical abundances in nearby galaxies possibly involved in the encounter such as M96 and NGC 3384 (Oey & Kennicutt 1993; Sánchez-Blázquez et al. 2007).

Based on observations collected at the European Southern Observatory under ESO programme 0104.A-0096(A). E.C. acknowledges support from PRIN MIUR 2017–20173*ML3WW*$_0$0 and Mainstream-GasDustpedia. G.V. acknowledges support from ANID programs FONDECYT Postdoctorado 3200802 and Basal-CATA AFB-170002.

ORCID iDs

Edvige Corbelli https://orcid.org/0000-0002-5788-2628
Giovanni Cresci https://orcid.org/0000-0002-5281-1417
Filippo Mannucci https://orcid.org/0000-0002-4803-2381
David Thilker https://orcid.org/0000-0002-8528-7340
Giacomo Venturi https://orcid.org/0000-0001-8349-3055

References

Asplund, M., Grevesse, N., Sauval, A. J., & Scott, P. 2009, ARA&A, 47, 481
Baldwin, J. A., Phillips, M. M., & Terlevich, R. 1981, PASP, 93, 5

Bekki, K., Koribalski, B. S., Ryder, S. D., & Couch, W. J. 2005, MNRAS, 357, L21
Boquien, M., Duc, P. A., Braine, J., et al. 2007, A&A, 467, 93
Bot, C., Helou, G., Latter, W. B., et al. 2009, AJ, 138, 452
Bruzual, G., & Charlot, S. 2003, MNRAS, 344, 1000
Byler, N., Dalcanton, J. J., Conroy, C., & Johnson, B. D. 2017, ApJ, 840, 44
Chabrier, G. 2003, PASP, 115, 763
Corbelli, E., Mannucci, F., Thilker, D., Cresci, G., & Venturi, G. 2021, A&A, submitted (Paper II)
Curti, M., Mannucci, F., Cresci, G., & Maiolino, R. 2020, MNRAS, 491, 944
Donahue, M., Aldering, G., & Stocke, J. T. 1995, ApJL, 450, L45
Dopita, M. A., Sutherland, R. S., Nicholls, D. C., Kewley, L. J., & Vogt, F. P. A. 2013, ApJS, 208, 10
Ghosh, K. K., & Mapelli, M. 2008, MNRAS, 386, L38
Kauffmann, G., Heckman, T. M., Tremonti, C., et al. 2003, MNRAS, 346, 1055
Kibblewhite, E. J., Cawson, M. G. M., Disney, M. J., & Phillipps, S. 1985, MNRAS, 213, 111
Leitherer, C., Schaerer, D., Goldader, J. D., et al. 1999, ApJS, 123, 3
Longmore, A. J., Hawarden, T. G., Cannon, R. D., et al. 1979, MNRAS, 188, 285
Maeder, A. 1992, A&A, 264, 105
Meynet, G., & Maeder, A. 2002, A&A, 390, 561
Michel-Dansac, L., Duc, P.-A., Bournaud, F., et al. 2010, ApJL, 717, L143
Mihos, J. C., Carr, C. T., Watkins, A. E., Oosterloo, T., & Harding, P. 2018, ApJL, 863, L7
Oey, M. S., & Kennicutt, R. C. J. 1993, ApJ, 411, 137
Pellegrini, E. W., Rahner, D., Reissl, S., et al. 2020, MNRAS, 496, 339
Pierce, M. J., & Tully, R. B. 1985, AJ, 90, 450
Reynolds, R. J., Magee, K., Roesler, F. L., Scherb, F., & Harlander, J. 1986, ApJL, 309, L9
Romano, D., Karakas, A. I., Tosi, M., & Matteucci, F. 2010, A&A, 522, A32
Rood, H. J., & Williams, B. A. 1985, ApJ, 288, 535
Rosenberg, J. L., Haislmaier, K., Giroux, M. L., Keeney, B. A., & Schneider, S. E. 2014, ApJ, 790, 64
Salpeter, E. E. 1955, ApJ, 121, 161
Sánchez-Blázquez, P., Forbes, D. A., Strader, J., Brodie, J., & Proctor, R. 2007, MNRAS, 377, 759
Sanders, N. E., Caldwell, N., McDowell, J., & Harding, P. 2012, ApJ, 758, 133
Schneider, S. 1985, ApJL, 288, L33
Schneider, S. E., Helou, G., Salpeter, E. E., & Terzian, Y. 1983, ApJL, 273, L1
Schneider, S. E., Salpeter, E. E., & Terzian, Y. 1986, AJ, 91, 13
Schneider, S. E., Skrutskie, M. F., Hacking, P. B., et al. 1989, AJ, 97, 666
Searle, L., & Sargent, W. L. W. 1972, ApJ, 173, 25
Sil'chenko, O. K., Moiseev, A. V., Afanasiev, V. L., Chavushyan, V. H., & Valdes, J. R. 2003, ApJ, 591, 185
Thilker, D. A., Donovan, J., Schiminovich, D., et al. 2009, Natur, 457, 990
Vilchez, J. M., & Esteban, C. 1996, MNRAS, 280, 720
Vincenzo, F., Matteucci, F., Belfiore, F., & Maiolino, R. 2016, MNRAS, 455, 4183
Watkins, A. E., Mihos, J. C., Harding, P., & Feldmeier, J. J. 2014, ApJ, 791, 38
Weilbacher, P. M., Palsa, R., Streicher, O., et al. 2020, A&A, 641, A28